REPORT DOCUMENTATION PAGE

Form Approved OMB No. 0704-0188

1. REPORT DATE *(DD-MM-YYYY)*	2. REPORT TYPE	3. DATES COVERED *(From - To)*
30-06-2003	Technical Paper	

4. TITLE AND SUBTITLE

Ion Energy Diagnostics in the Far-Field Plume of a High-Specific Impulse Hall Thruster

5a. CONTRACT NUMBER

5b. GRANT NUMBER

5c. PROGRAM ELEMENT NUMBER

6. AUTHOR(S)

Richard R. Hofer (QSS Group); James M. Haas (AFRL/PRSS); Alec D. Gallimore (Univ. of Michigan)

5d. PROJECT NUMBER
1011

5e. TASK NUMBER
0009

5f. WORK UNIT NUMBER

7. PERFORMING ORGANIZATION NAME(S) AND ADDRESS(ES)

Air Force Research Laboratory (AFMC)
AFRL/PRSS
1 Ara Drive
Edwards AFB CA 93524-7013

8. PERFORMING ORGANIZATION REPORT NUMBER

AFRL-PR-ED-TP-2003-177

9. SPONSORING / MONITORING AGENCY NAME(S) AND ADDRESS(ES)

Air Force Research Laboratory (AFMC)
AFRL/PRS
5 Pollux Drive
Edwards AFB CA 93524-7048

10. SPONSOR/MONITOR'S ACRONYM(S)

11. SPONSOR/MONITOR'S NUMBER(S)
AFRL-PR-ED-TP-2003-177

12. DISTRIBUTION / AVAILABILITY STATEMENT

Approved for public release; distribution unlimited.

13. SUPPLEMENTARY NOTES

For presentation at the AIAA Joint Propulsion Conference in Huntsville, AL, taking place 20-23 July 2003.

14. ABSTRACT

15. SUBJECT TERMS

16. SECURITY CLASSIFICATION OF:			17. LIMITATION OF ABSTRACT	18. NUMBER OF PAGES	19a. NAME OF RESPONSIBLE PERSON
a. REPORT	b. ABSTRACT	c. THIS PAGE			Leilani Richardson
Unclassified	**Unclassified**	**Unclassified**	A	12	19b. TELEPHONE NUMBER *(include area code)* (661) 275-5015

Ion energy diagnostics in the far-field plume of a high-specific impulse Hall thruster

Richard R. Hofer*
QSS Group, Inc.
Cleveland, OH 44135 USA
richard.hofer@grc.nasa.gov

James M. Haas*
Air Force Research Laboratory
Edwards Air Force Base, CA 93524 USA

Alec D. Gallimore†
Plasmadynamics and Electric Propulsion Laboratory
University of Michigan
Ann Arbor, MI 48109 USA

ABSTRACT

Retarding potential analyzer and cylindrical Langmuir probe measurements were taken on the laboratory model NASA-173Mv2 to improve understanding of the physical processes affecting Hall thruster performance at high specific impulse. A retarding potential analyzer was used to measure the ion voltage distribution at voltages of 300-800 V. A cylindrical Langmuir probe was also used to obtain the local plasma potential so that the true ion voltage was obtained. The goal of the experiments was to provide information on the ionization and acceleration processes internal to the thruster as a function of discharge voltage and magnetic field. The results have shown that the ratio of ion energy to discharge voltage and the width of the ion voltage distribution both increased with discharge voltage. This implied that the primary ionization zone was growing in axial extent and moving closer to the anode as the discharge voltage increased.

I. INTRODUCTION

As used for spacecraft applications in Earth orbit such as station-keeping, orbit-raising, and orbit-transfers, the xenon-fueled Hall thruster is generally regarded as a 1600 second specific impulse (Isp) device that operates at discharge voltages of 300 V. Mission studies have shown though that moderate increases in the Isp of Hall thrusters to the 2000-3000 second range can enhance or enable a number of Earth-orbital and interplanetary missions.[1-6]

The NASA-173M series of laboratory-model Hall thrusters were conceived to understand the design challenges and physical mechanisms determining performance in the 2000-3000 second range of Isp.[7-10] The basic philosophy underlying their designs was that changes to the magnetic field topography would be required for efficient operation above 300 V. Advanced magnetic circuits allowing for *in situ* variation of the field topography were therefore incorporated into each thruster. The NASA-173Mv1, built jointly by the University of Michigan and the NASA Glenn Research Center (GRC), established the validity of this approach.[7-8] In a performance study at low current densities, changes to the magnetic field topography at high-voltage were shown to be critical to achieving efficient operation.[8] The follow-on design developed at GRC, the NASA-173Mv2, was fabricated to incorporate design improvements suggested by its predecessor. A performance mapping of the 173Mv2 at several current densities established that efficient operation in the 2000–3000 second range of Isp was possible if a minimum current density was maintained and the magnetic field topography was properly shaped.[9]

Design and experiment has established the feasibility of operating Hall thrusters efficiently at high-Isp. A need exists, however, to establish a more fundamental relationship between the thruster design and the microscopic plasma properties so that higher-fidelity thrusters can be engineered. This is necessary to further improve performance, establish an understanding of lifetime, and enable integration with spacecraft. A comprehensive series of plasma diagnostics have therefore been deployed on the NASA-173Mv2 to

* Research Scientist, Member AIAA
* Associate Professor, Associate Fellow AIAA

improve basic understanding of the plasma characteristics. Previous studies have considered plume divergence, plasma oscillations, internal floating potential, and very-near-field ion current density.[9-10]

In the present work, a retarding potential analyzer was used to measure the ion voltage distribution of the NASA-173Mv2 on thruster centerline, two meters downstream of the exit plane, at a constant xenon flow rate of 10 mg/s and voltages of 300-800 V. A cylindrical Langmuir probe was also used to obtain the local plasma potential so that the true ion voltage was obtained. The goal of the experiments was to provide information on the ionization and acceleration processes internal to the thruster as a function of discharge voltage and magnetic field. The results have shown that the ratio of ion energy to discharge voltage and the width of the ion voltage distribution both increased with discharge voltage. This implied that the primary ionization zone was growing in axial extent and moving closer to the anode as the discharge voltage increased.

II. EXPERIMENTAL APPARATUS

The hardware used in these experiments were identical to those used in the performance and plume characterization described in Ref. 9. This includes the thruster, power electronics, vacuum facility, and how the thruster was mounted in the vacuum facility. The only changes were the addition of the Langmuir probe and retarding potential analyzer.

A. NASA-173Mv2 Hall effect thruster

The laboratory model NASA-173Mv2 is a 5 kW-class Hall thruster that has a discharge chamber outer diameter of 173 mm (Figure 1; see Ref. 9 for a detailed description). A fixed structure of magnetic poles pieces, an inner coil (IC) and an outer coil (OC) are used to form the primary magnetic circuit. Fine control of the magnetic field is provided with an internal trim coil (ITC) and an external trim coil (ETC). The ITC primarily affects the radial magnetic field in the discharge chamber, while the ETC affects the magnetic field downstream of the exit plane and near the cathode. Operation without the ITC or ETC is referred to as "+IC, +OC," meaning that only the IC and OC were used. The symbols "+" or "-" indicate the polarity of a coil, where "+" adds and "-" subtracts from the magnetic field.

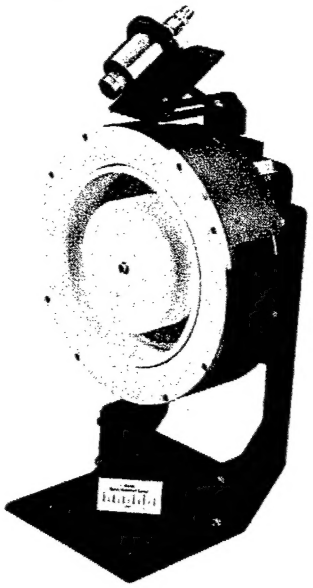

Figure 1 - Photograph of the NASA-173Mv2 Hall thruster.

Figure 2 shows the total specific impulse and total efficiency of the NASA-173Mv2 at 10 mg/s versus discharge voltage. The data is from the performance characterization of Ref. 9. The Isp and efficiency include cathode flow and the efficiency also includes the power to operate the magnets. Isp and efficiency ranges from 1600-3400 seconds and 51-61%, respectively, over the voltage range of 300-1000 V. Trim coils always improved efficiency by 1-2%.

The plasma discharge was powered by a matching pair of commercially available power supplies wired in series that provided a 1200 V, 16 A output. The discharge filter consisted of a 100 μF capacitor in parallel with the supply outputs. Other commercially available power supplies were used to power the magnet coils and the cathode heater and keeper. The hollow cathode was a 20 A laboratory model fabricated at GRC and positioned above the thruster (see Figure 1).

Xenon (99.999% pure) was supplied through stainless steel feed lines with 20 and 200 sccm mass flow controllers. The controllers were calibrated before the experiments using a constant-volume method. The estimated uncertainty of the calibrations was ±0.7% for the anode and ±1.4% for the cathode.

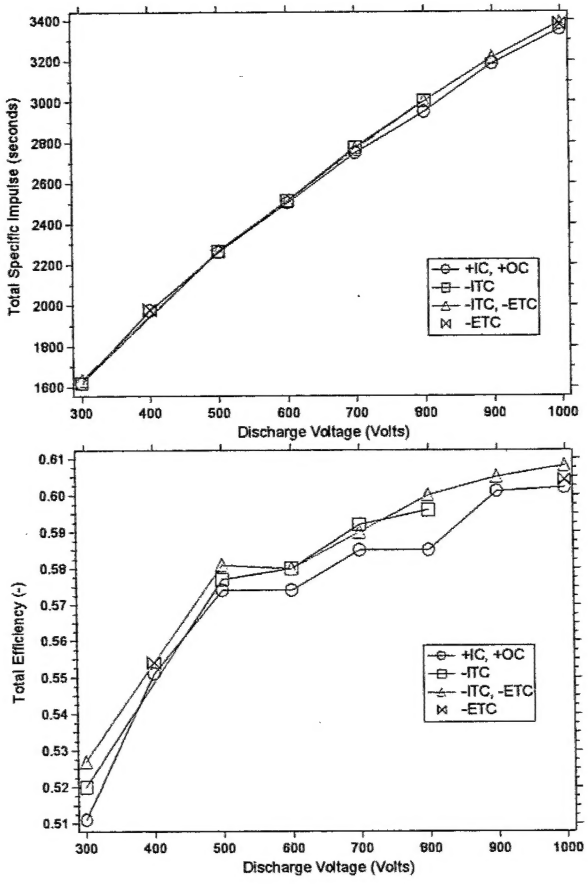

Figure 2 - Total specific impulse and efficiency versus discharge voltage of the NASA-173Mv2 at 10 mg/s (from Ref. 9).

Thruster telemetry was acquired using a 22-bit datalogger. The DC accuracy of the unit, as reported by the manufacturer, is 0.004%. However, calibration of each channel using digital multimeters increased the uncertainty to ±0.05% for voltage and ±0.2% for current.

The thruster was operated for four hours after initial exposure to vacuum conditions to allow for outgassing of the chamber walls. Upon subsequent thruster shutdowns and restarts or a change in the discharge voltage, the 173Mv2 was operated for at least 30-60 minutes before data was acquired. This allowed enough time for the discharge current to reach a steady-state value.

B. Vacuum facility

All experiments were conducted in vacuum facility 12 (VF12) at GRC. VF12 is a cylindrical, stainless steel chamber 3.0 m in diameter by 9.6 meters in length. The facility is cryogenically pumped and backed by a turbomolecular pump for removal of low molecular weight gases that are not pumped by the cryosurfaces. The thruster was mounted on the thrust stand described in Ref. 9. The thrust stand was locked down and was not used for these experiments. In this position, the thruster was near the chamber's centerline on one end of the facility and fired 8.9 m down the length of the tank toward the pumps, which are located along the back half of the chamber. A hot-cathode ionization gauge was mounted 0.4 m below the vertical chamber centerline, 5.2 m downstream from the thruster. Pressure measurements were corrected for xenon using the base pressure on air and a correction factor of 2.87 for xenon. For xenon flow rates of 1 and 10 mg/s through the anode and cathode, respectively, the pressure was 4.6×10^{-6} Torr, after correcting for xenon and the base pressure on air, which was 1.0×10^{-7} Torr. This corresponded to an average xenon pumping rate of 340,000 l/s.

C. Cylindrical Langmuir probe

A cylindrical Langmuir probe was used to estimate the plasma potential (V_p) with respect to facility ground near the location of the RPA. As described in the next section, Vp was needed to obtain the true ion voltage. The measurements were taken during other experiments with an ExB probe.

The Langmuir probe had a diameter of 1.60 mm and a length of 16.5 mm. The length of the probe was aligned parallel to the ion flow, with the mid-point located 2 m downstream of the thruster exit plane and 62 mm radially from thruster centerline. The estimated uncertainty in the plasma potential because the Langmuir probe was not on centerline (where the RPA was actually located) was less than one volt.[11]

The magnetic field leaking from the permanent magnets in the ExB probe was on the order of a few Gauss. This was sufficiently small that the magnetic field could be neglected in the analysis of the probe characterstic.

The plasma potential was found from the maximum in the first derivative of the electron current. This method is convenient because it is easily automated in the data analysis, but tends to underestimate the plasma potential when compared to graphical analysis using curve fitting.[12] Comparisons between the different

methods on a few test cases showed that the derivative method was consistently lower than the graphical method by a value on the order of a volt.

Considering all sources of error described above, the uncertainty in the plasma potential was estimated to be +2/-1 V.

D. Retarding potential analyzer

The retarding potential analyzer (RPA) allows the collection of selectively filtered ions by applying a retarding potential across an inlet grid. The RPA acts as a high-pass filter, that is, for a given grid potential, only ions with energy to charge ratios (E/q) greater than the grid voltage pass and reach a collection electrode. The derivative of the resulting current-voltage characteristic, dI/dV, is proportional to the ion voltage distribution:

$$\frac{dI}{dV} = -\frac{q_i^2 e^2 n_i A_c}{m_i} f(V) \qquad (1)$$

(where q_i is the charge-state of the ion, e is the elementary charge, n_i is the ion density, A_c is the probe collection area, m_i is the ion mass, and f(V) is the ion voltage distribution function).[13] Note that the RPA measures the ion energy distribution only if the plasma is composed of ions of the same mass and charge. This is not the case for Hall thrusters, which for 300 V discharges are known to be composed of 7-11% Xe2+ and <1% Xe3+.[11,13] As a result, the RPA measures the ion voltage distribution function when used with Hall thrusters.

The RPA used in these experiments was based on the multi-gridded energy analyzer design of Hutchinson.[14] It is composed of three grids and shown schematically in Figure 3. The outer body of the RPA is constructed of 316 stainless steel (SS) tubing, which was held at ground potential. A phenolic sleeve placed inside the body provides electrical isolation of the grids. All grids are identical and are cut from 316 SS, photochemically machined sheet with a thickness of 0.005". The grid openings are 0.011" diameter with a total open area fraction of 38%. Grid spacing is achieved using machinable glass-mica ceramic washers, fabricated to provide the correct separation distances. The collector is a copper disk. Electrical connections are accomplished by spot welding stainless steel wire to each grid. The wires are then routed along the inner edge of the phenolic sleeve and out the rear of the body. The washers and grids are fixed in place by a spring placed behind the collector and fixed in place by a rear cover. Relevant dimensions are summarized in Table 1.

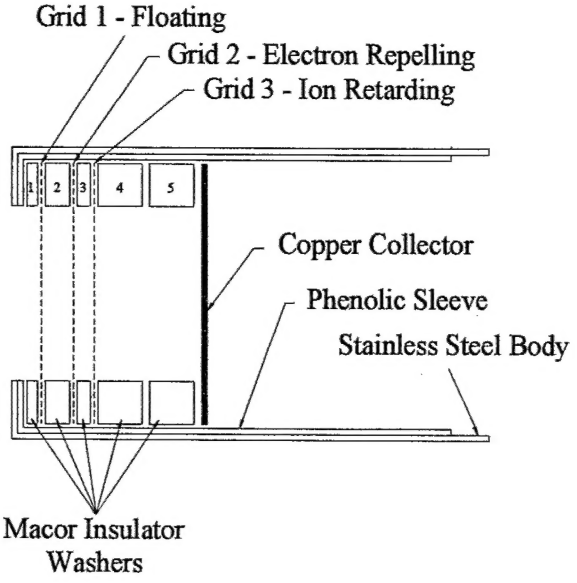

Figure 3 - Schematic of the RPA.

Table 1 - RPA washer thicknesses and inner diameters.

Washer	Thickness	I.D.
1	0.038"	0.733"
2	0.132"	0.851"
3	0.068"	0.853"
4	0.257"	0.842"
5	0.257"	0.845"

During operation, grid 1 floated to minimize perturbation between the probe and ambient plasma while grid 2 was biased -30 V below ground to repel incident electrons. Grid 3 was swept over voltages ranging from 0 to 1100 V relative to ground using a sourcemeter. The ion current to the collector was measured using a picoammeter. Figure 4 shows the RPA electrical

schematic.

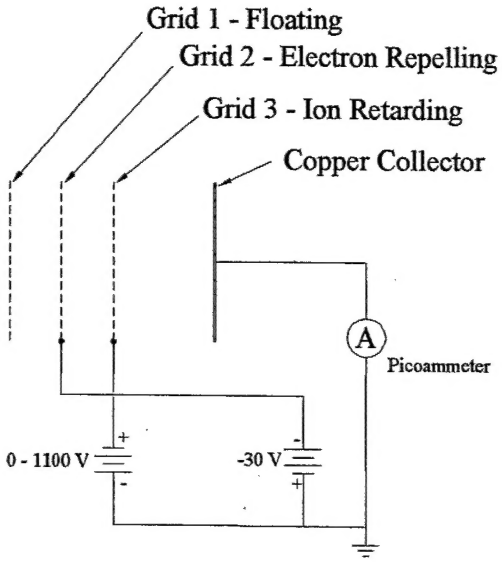

Figure 4 - RPA electrical schematic.

The RPA measures the ion energy-to-charge ratio (i.e., the ion voltage) with respect to facility ground. As shown in the potential diagram of Figure 5, the true ion voltage (V_{true}) is obtained if the plasma potential is subtracted from the measured value (V_{rpa}).

$$V_{true} = V_{rpa} - V_p \qquad (2)$$

It is also convenient to define the loss voltage (V_{loss}) as the difference between the discharge voltage (V_d) and true ion voltage.

$$V_{loss} = V_d - V_{true} \qquad (3)$$

In Ref. 15, the ion voltage distributions measured by the RPA were compared to a 45° parallel-plate electrostatic energy analyzer (ESA) by Beal, et al. These experiments were conducted 0.5 m downstream of the BHT-200-X3 Hall thruster as a function of angular position. Figure 6 compares the distributions measured by the RPA and the ESA on thruster centerline. Voltage was measured with respect to facility ground. The peak ion voltage measured by the two diagnostics was found to agree within 8 V for a 220 V discharge, or 3.6%. As stated by the authors, the peak ion voltage should be more accurate because it is much less sensitive to instrument misalignment than the ESA. The wide disparity between the width of the distributions from the two diagnostics is thought to be due to instrument broadening. The acceptance angle of the ESA was 4° compared to 45° in the RPA. As a result, the width of the ion voltage distribution is more accurate in the ESA.

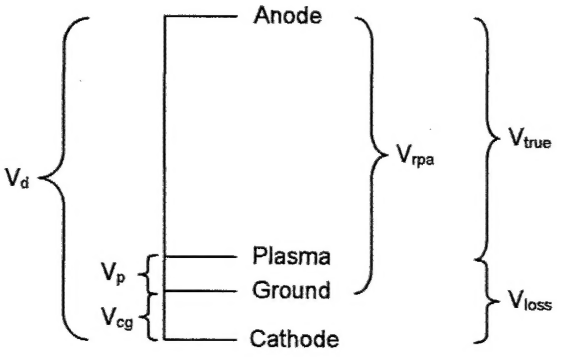

Figure 5 - Potential diagram showing the relationship between the measured quantities (V_{rpa}, V_p), the true ion voltage (V_{true}), and the loss voltage (V_{loss}).

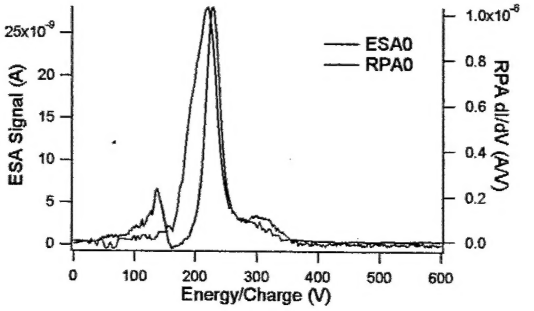

Figure 6 - Ion voltage distributions measured with the RPA and a parallel-plate energy analyzer on the centerline of the BHT-200-X3, 0.5 m downstream of the exit plane. (from Ref. 15)

III. RESULTS

Langmuir probe and RPA measurements were taken during separate testing periods with the thruster operating at an anode flow rate of 10.0 mg/s and a cathode flow rate of 1.0 mg/s. Langmuir probe measurements tested discharge voltages of 300-1000 V, while the RPA measurements spanned discharge voltages of 300-800 V. A grid short with the RPA ended testing prematurely at 800 V. At each discharge voltage, the effects of the magnetic field were evaluated by operating at several different combinations of the thruster coils. These were without the trim coils (+IC,+OC), with the internal trim coil (-ITC), with both the internal and external trim coils, (-ITC,-ETC), and with the external trim coil (-ETC).

Thruster telemetry for both test series are tabulated in the appendix.

A. Plasma potential

Figure 7 plots the plasma potential with respect to facility ground versus the discharge voltage for several magnetic field configurations. The plasma potential was found to increase by three volts as the discharge voltage increased from 300-1000 V, regardless of the magnetic field configuration. It was found that operating the ETC dropped the plasma potential by 1-2 V at each discharge voltage. The ITC had no effect on the plasma potential. The plasma potential data was used to correct the RPA ion voltage distributions so that the true ion voltage could be computed.

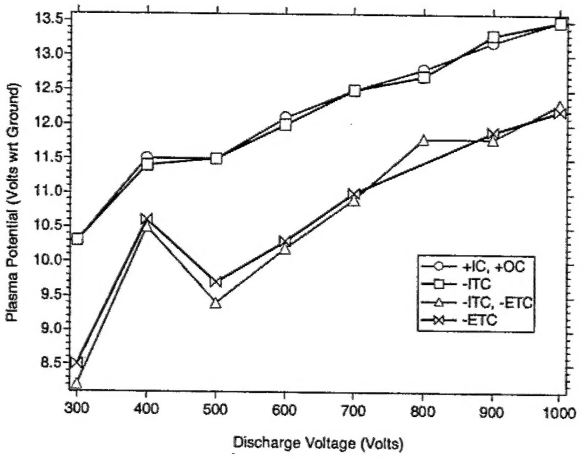

Figure 7 - Plasma potential versus discharge voltage for several magnetic field configurations, two meters downstream from the thruster exit plane. The external trim coil (ETC) lowered the plasma potential by 1-2 volts.

B. Ion voltage distribution

At each discharge voltage and magnetic field, three sweeps of the ion retarding voltage were performed with the RPA. The I-V curves from the RPA were found to be highly repeatable. Figure 8 shows the raw data from voltage sweeps when the inner and outer coils where energized (+IC, +OC). Except for 800 V (where a grid short occurred after one sweep), each curve in Figure 8 consists of the data from three separate sweeps. Before differentiating the data to obtain the ion voltage distribution, the data from each sweep were averaged together.

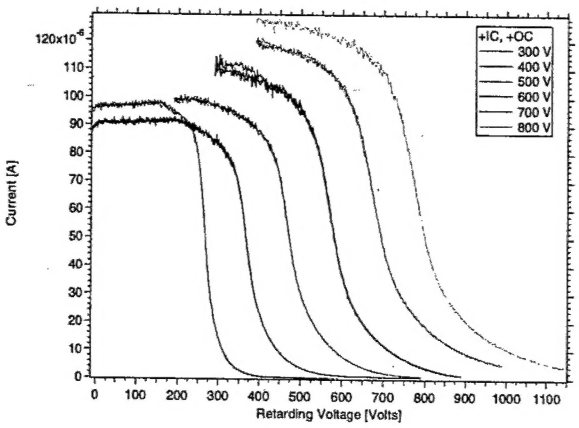

Figure 8 - Ion current versus retarding voltage from the RPA. The inner coil (+IC) and outer coil (+OC) are energized, no trim coils are used. To demonstrate repeatability, data from several sweeps are shown for each voltage, except 800 V where only one sweep was obtained.

To obtain the ion voltage distribution, the averaged data from each discharge voltage and magnetic field configuration was numerically differentiated. This induced a significant amount of numerical noise. To smooth the signal, the differentiated data was fit using a smoothing spline algorithm.[10] The raw data and the spline are compared for discharge voltages of 300 and 700 V (+IC, +OC) in Figure 9. The spline operation induced enough smoothing that detailed features from charge-exchange or elastic collisions were difficult to discern. As a result, the RPA ion voltage distributions were used only to compute the peak ion voltage and the width of the distribution. The peak ion voltage was relatively insensitive to the smoothing parameters. The uncertainty in the peak ion voltage was estimated as ±0.5%. The width of the ion voltage distribution was characterized by the full-width at half-maximum (FWHM). The FWHM was found to be more sensitive to the smoothing parameters than the peak ion voltage. The uncertainy in the FWHM was estimated as ±1% of the discharge voltage. The uncertainty estimates were based on numerical experiments that examined how the peak ion voltage and FWHM depended on the smoothing paramters.

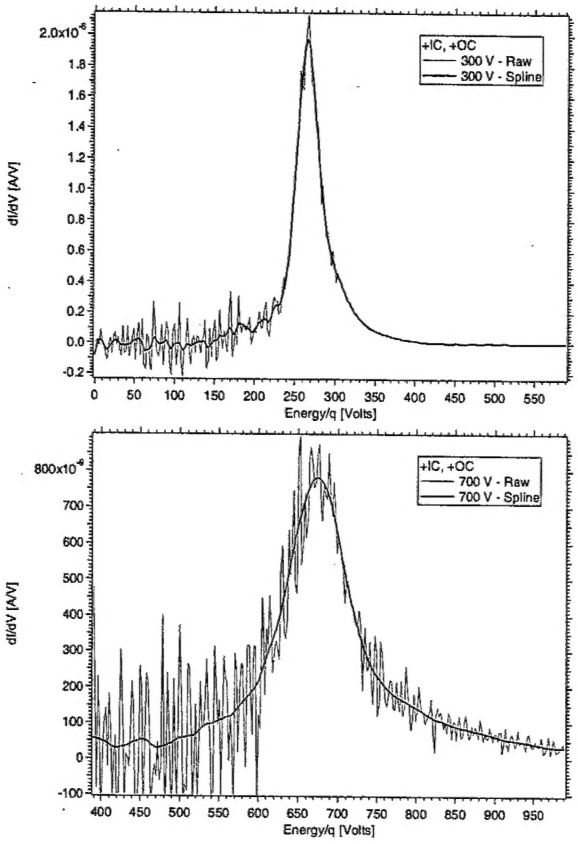

Figure 9 - The first derivative of the RPA I-V characteristic versus ion voltage. Both the raw data and the cubic spline of the data are shown for discharge voltages of 300 and 700 V (+IC, +OC).

Figure 10 shows the ion voltage distribution (normalized to the peak ion current) at each discharge voltage and magnetic field configuration. The distributions were similar in shape regardless of the discharge voltage, the most notable difference being an increase in the FWHM as the discharge voltage increased.

From each of the distributions in Figure 10 the loss voltage and the FWHM were calculated. Figure 11 shows the loss voltage while Figure 12 shows the FWHM as functions of the discharge voltage and magnetic field. The loss voltage decreased with discharge voltage from 35 V at 300 V to 25 V at 800 V. There was no systematic dependance of the loss voltage with the magnetic field. The FWHM increased with discharge voltage from 35 V at 300 V to 105 V at 800 V. The use of the ETC decreased the FWHM by about 5 V when it was used.

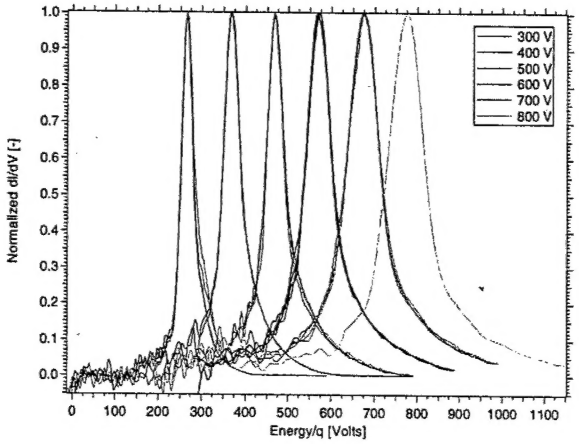

Figure 10 - Normalized ion voltage distributions at each discharge voltage for each magnetic field configuration.

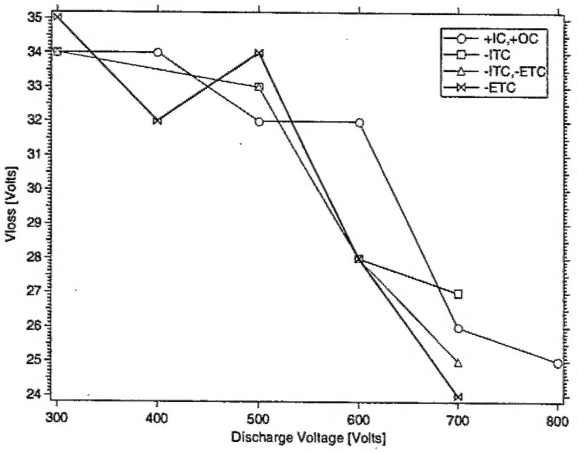

Figure 11 - Loss voltage versus the discharge voltage with different magnetic field configurations.

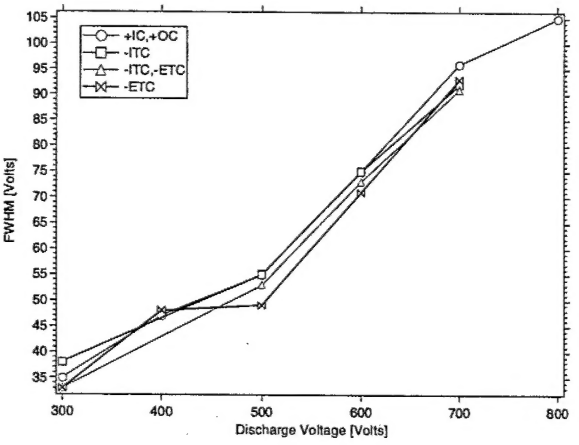

Figure 12 - The full-width at half-maximum (FWHM) of the ion voltage distributions versus discharge voltage with different magnetic field configurations.

IV. DISCUSSION

A. Plasma potential

The primary purpose of the plasma potential measurements was to shift the ion voltage distributions so that the true ion voltage could be found. Figure 7 shows that the plasma potential ranged from 8.5-13.5 V. While still a small fraction of the discharge voltage, the plasma potential was a significant fraction of the loss voltage, which ranged from 25-35 V. The measurements emphasize the importance of obtaining the true ion voltage if an accurate measurement of the loss voltage is desired.

A remarkable feature of Figure 7 is the 1-2 V drop in plasma potential caused by the ETC. At 400 V, the plasma potential drop was smaller than the other discharge voltages because the ETC was energized to -2 A. All other discharges voltages used a coil current of -4 to -6 A. The trends indicate that the drop in plasma potential was independent of the ion energy. The drop in plasma potential was unexpected for two reasons. First, because the Langmuir probe was two meters from the thruster it was expected that any differences caused by the magnetic field near the thruster would have been smoothed out. Second, the ETC altered the magnetic field by a relatively small amount. Measurements with a hand-held Gaussmeter showed that the magnetic field decreased only by a few Gauss when the ETC was energized to -5 A.

The drop in plasma potential was consistent with numerical modeling by Keidar, who showed that a decreasing magnetic field would decrease the plasma potential.[17] The drop in plasma potential could be important in controlling the charge-exchange plasma near the thruster, which is known to cause erosion of sensitive spacecraft surfaces.

B. Ion voltage distribution

The RPA is an important plasma diagnostic because it yields information on the voltage distributuion of ions emanating from the thruster. This information is needed by spacecraft designers to calculate plume impingement on sensitive surfaces such as solar arrays and optics. Knowledge of the ion voltage distribution is also important to thruster design. The spread in ion voltage and their mean energy are critical to both maximizing life and optimizing performance. However, charge-exchange and elastic collisions and axial variations of the plasma potential in the plume can change the distributions as the plume propagates from the thruster. These changes manifest themselves through collision signatures (broadening or secondary peaks) or shifts in the distribution caused by electric fields. These effects can be minimized by operating at low pressures or corrected for through secondary measurements (such as the axial variation of the plasma potential). As a result of these plume effects, the data from the RPA was used primarily to analyze the relative variations between operating conditions (discharge voltage and magnetic field).

From Figure 11, the loss voltage was shown to decrease with increasing discharge voltage. A decrease in the loss voltage meant that the acceleration efficiency,

$$\eta_a = \frac{\langle \varepsilon_i \rangle}{eV_d} \qquad (4)$$

(where $\langle \varepsilon_i \rangle$ is the mean ion energy) increased.[18] An increase in the acceleration efficiency could result if either (or both) the acceleration layer or ionization zone moved closer to the anode. Internal measurements of the floating potential from Ref. 10 indicated that the acceleration layer moved closer to the anode as the discharge voltage increased. Visual observations of the brightness of the plasma in the discharge chamber have also indicated that the plasma moved closer to the anode, which implied a movement in the ionization zone. Taken together, the various measurements imply that both the acceleration layer and the ionization zone were moving closer to the anode with discharge voltage. The end result was an increase in the mean ion energy and therefore increased acceleration efficiency.

From Figure 12, the FWHM was shown to increase with increasing discharge voltage. An increase in the FWHM meant that the dispersion efficiency,

$$\eta_d = \frac{\langle U_i \rangle^2}{\langle U_i^2 \rangle} \qquad (5)$$

(where U_i is the ion velocity) decreased.[18] The dispersion efficiency characterizes the spread in ion velocities (or energy). The dispersion efficiency will decrease if either (or both) the acceleration layer or ionization zone grow thicker in the axial direction. Internal measurements of the floating potential from Ref. 10 did not indicate that the thickness of the acceleration layer was growing. This implies that the ionization zone simply increased in length as the discharge voltage increased.

The conclusion reached was that increased discharge voltage resulted in a thickening of the ionization zone and a translation towards the anode. This could occur if the average electron temperature remains above the ionization potential over a greater axial extent. Such a situation is consistent with increases in the discharge voltage, because the ability of the walls to moderate the electron temperature decreases with discharge voltage. The end result of increased ionization zone thickness was an increase in the average ion energy and a wider distribution of ion energies. This could be undesirable from the standpoint of lifetime because it implies a greater number of ion impacts with the walls. However, because the performance of the thruster was still favorable, the increase in erosion may have been second order. Other off-axis effects may have contributed to better focussing of the ion beam with discharge voltage, such as the curvature of the magnetic field lines. This hypothesis was consistent with the observed decrease in plume divergence from Ref. 9 from 38° to 28° over voltages of 300-1000 V.

ACKNOWLEDGEMENTS

Support of this research by the NASA Glenn Research Center through grant NAG3-2307 (David Jacobson, technical monitor) is greatly appreciated.

REFERENCES

1. Deininger, W. D., "Advanced Propulsion System Options for Geostationary Satellites," AIAA-94-3001, June 1994.
2. Oleson, S. R., "Electric Propulsion for Low Earth Orbit Communications Satellites," IEPC-97-102, 25th International Electric Propulsion Conference, Cleveland, OH, Aug 24-28, 1997.
3. Oleson, S. R., Myers, R. M., "Advanced Propulsion for Geostationary Orbit Insertion and North-South Station Keeping," Journal of Spacecraft and Rockets, Vol. 34, No. 1, pp. 22-28, Jan-Feb 1997.
4. Gefert, L. P., Hack, K. J., "Options for the Human Exploration of Mars Using Solar Electric Propulsion," AIP Conference Proceedings, No. 458, pp. 1275-1280, STAIF-99, Nov 1999.
5. Oleson, S. R., Benson, S. W., "Electric Propulsion for International Space Station Reboost: A Fresh Look," AIAA-2001-3644, 37th Joint Propulsion Conference, Salt Lake City, UT, July 8-11, 2001.
6. Oleson, S. R., "Mission Advantages of Constant Power, Variable Isp Electrostatic Thrusters," AIAA-2000-3413, 36th Joint Propulsion Conference, Huntsville, AL, July 17-19, 2000.
7. Hofer, R. R., Peterson, P. Y., Gallimore, A. D., "A High Specific Impulse Two-Stage Hall Thruster with Plasma Lens Focusing," IEPC-01-036, 27th International Electric Propulsion Conference, Pasadena, CA, Oct 14-19, 2001.
8. Hofer, R. R., Gallimore, A. D., "The Role of Magnetic Field Topography in Improving the Performance of High-Voltage Hall Thrusters," AIAA-2002-4111, 38th Joint Propulsion Conference, Indianapolis, IN, July 7-10, 2002.
9. Hofer, R. R., Jankovsky, R. S., "The Influence of Current Density and Magnetic Field Topography in Optimizing the Performance, Divergence, and Plasma Oscillations of High Specific Impulse Hall Thrusters," IEPC-03-142, 28th International Electric Propulsion Conference, Toulouse, France, March 17-21, 2003.
10. Hofer, R. R., Gallimore, A. D., "Recent Results from Internal and Very-Near-Field Plasma Diagnostics of a High Specific Impulse Hall Thruster," IEPC-03-037, 28th International Electric Propulsion Conference, Toulouse, France, March 17-21, 2003.
11. Gulczinski, F.S., "Examination of the Structure and Evolution of Ion Energy Properties of a 5 kW Class Laboratory Hall Effect Thruster at Various Operational Conditions," Ph.D. Dissertation, University of Michigan, 1999.

12. Lochte-Holtgreven, W., ed., Plasma Diagnostics, American Elsevier Publishing, New York, 1968.
13. King, L.B., "Transport-property and Mass Spectral Measurements in the Plasma Exhaust Plume of a Hall-effect Space Propulsion System," Ph.D. Dissertation, University of Michigan, 1998.
14. Hutchinson, I. H., Principles of Plasma Diagnostics, Cambridge University Press, New York, 2002.
15. Beal, B. E., Gallimore, A. D., "Energy Analysis of a Hall Thruster Cluster," IEPC-03-35, 28th International Electric Propulsion Conference, Toulouse, France, March 17-21, 2003.
16. Reinsch, Christian H., "Smoothing by Spline Functions," Numerische Mathematic 10, pp. 177-183, 1967.
17. Keidar, M., Boyd, I. D., "Effect of a Magnetic Field on the Plasma Plume from Hall Thrusters," Journal of Applied Physics, Vol. 86, No. 9, November 1, 1999.
18. Kim, V., "Main Physical Features and Processes Determining the Performance of Stationary Plasma Thrusters," Journal of Propulsion and Power, Vol. 14, No. 5, Sept-Oct, 1998, pp. 736-743.

APPENDIX

Table 2 - NASA-173Mv2 telemetry from Langmuir probe measurements.

Point	Vd (V)	Id (A)	Anode (mg/s)	Cathode (mg/s)	Inner Coil (A)	Outer Coil (A)	Internal Trim Coil (A)	External Trim Coil (A)	Vcg (V)	Pressure (Torr)
148	300.3	9.00	10.00	1.00	1.75	1.50	0.00	0.00	-11.3	4.6E-06
149	300.4	8.89	10.00	1.00	1.75	1.50	-0.54	0.00	-11.2	4.6E-06
150	300.4	8.88	10.00	1.00	1.75	1.50	-0.54	-4.00	-10.6	4.6E-06
151	300.4	8.99	10.00	1.00	1.75	1.50	0.00	-4.00	-10.9	4.6E-06
152	400.2	9.32	10.00	1.00	2.50	2.26	0.00	0.00	-12.7	4.6E-06
153	400.2	9.26	10.00	1.00	2.50	2.26	-0.36	0.00	-12.7	4.6E-06
154	400.2	9.25	10.00	1.00	2.50	2.26	-0.36	-2.00	-12.3	4.6E-06
155	400.2	9.32	10.00	1.00	2.50	2.26	0.00	-2.00	-12.2	4.6E-06
156	500.3	9.49	10.00	1.00	3.00	2.20	0.00	0.00	-13.2	4.6E-06
157	500.3	9.34	10.00	1.00	3.00	2.20	-0.35	0.00	-13.4	4.6E-06
158	500.3	9.42	10.00	1.00	3.00	2.20	-0.35	-5.00	-12.7	4.6E-06
159	500.3	9.46	10.00	1.00	3.00	2.20	0.00	-5.00	-12.6	4.6E-06
160	600.3	9.41	10.00	1.00	3.26	2.49	0.00	0.00	-13.0	4.6E-06
161	600.3	9.24	10.00	1.00	3.26	2.49	-0.26	0.00	-13.5	4.6E-06
162	600.3	9.35	10.00	1.00	3.26	2.49	-0.26	-5.00	-12.9	4.6E-06
163	600.3	9.46	10.00	1.00	3.26	2.49	0.00	-5.00	-12.4	4.6E-06
164	700.3	9.40	10.00	1.00	3.41	3.06	0.00	0.00	-14.3	4.6E-06
165	700.3	9.53	10.00	1.00	3.41	3.06	-0.20	0.00	-14.1	4.6E-06
166	700.3	9.51	10.00	1.00	3.41	3.06	-0.20	-5.00	-13.8	4.6E-06
168	700.5	9.54	10.00	1.00	3.41	3.06	0.00	-5.00	-13.3	4.6E-06
170	800.1	9.44	10.00	1.00	3.82	3.30	0.00	0.00	-14.7	4.6E-06
171	800.1	9.55	10.00	1.00	3.82	3.30	-0.21	0.00	-14.5	4.6E-06
172	800.1	9.53	10.00	1.00	3.82	3.30	-0.21	-5.00	-13.9	4.6E-06
175	900.4	9.61	10.00	1.00	3.85	3.61	0.00	0.00	-13.8	4.6E-06
176	900.4	9.72	10.00	1.00	3.85	3.61	-0.04	0.00	-13.8	4.6E-06
177	900.4	9.73	10.00	1.00	3.85	3.61	-0.04	-5.90	-13.3	4.6E-06
178	900.4	9.73	10.00	1.00	3.85	3.61	0.00	-5.90	-13.3	4.6E-06
181	1000.1	9.71	10.00	1.00	4.36	3.81	0.00	0.00	-14.2	4.6E-06
182	1000.1	9.85	10.00	1.00	4.36	3.81	-0.16	0.00	-13.8	4.6E-06
183	1000.1	9.94	10.00	1.00	4.36	3.81	-0.16	-5.00	-13.1	4.6E-06
184	1000.1	10.08	10.00	1.00	4.36	3.81	0.00	-5.00	-12.9	4.6E-06

Table 3 - NASA-173Mv2 telemetry from RPA measurements.

Point	Vd (V)	Id (A)	Anode (mg/s)	Cathode (mg/s)	Inner Coil (A)	Outer Coil (A)	Internal Trim Coil (A)	External Trim Coil (A)	Vcg (V)	Pressure (Torr)
70	300.2	8.86	10.00	1.00	1.75	1.50	0.00	0.00	-11.9	4.6E-06
71	300.2	8.68	10.00	1.00	1.75	1.50	-0.54	0.00	-11.9	4.6E-06
72	300.1	8.68	10.00	1.00	1.75	1.50	-0.54	-4.00	-11.5	4.6E-06
73	300.2	8.88	10.00	1.00	1.75	1.50	0.00	-4.00	-11.5	4.6E-06
74	400.4	9.24	10.00	1.00	2.50	2.26	0.00	0.00	-12.7	4.6E-06
75	400.4	9.24	10.00	1.00	2.50	2.26	0.00	-2.00	-12.7	4.6E-06
76	500.4	9.38	10.00	1.00	3.00	2.20	0.00	0.00	-13.2	4.6E-06
77	500.3	9.23	10.00	1.00	3.00	2.20	-0.35	0.00	-13.1	4.6E-06
78	500.4	9.29	10.00	1.00	3.00	2.20	-0.35	-5.00	-13.1	4.6E-06
79	500.4	9.43	10.00	1.00	3.00	2.20	0.00	-5.00	-13.3	4.6E-06
82	600.3	9.53	10.00	1.00	3.26	2.49	0.00	0.00	-13.1	4.6E-06
83	600.3	9.47	10.00	1.00	3.26	2.49	-0.26	0.00	-12.8	4.6E-06
84	600.3	9.51	10.00	1.00	3.26	2.49	-0.26	-5.00	-12.5	4.6E-06
85	600.3	9.53	10.00	1.00	3.26	2.49	0.00	-5.00	-12.7	4.6E-06
86	700.1	9.68	10.00	1.00	3.41	3.06	0.00	0.00	-13.1	4.6E-06
87	700.1	9.62	10.00	1.00	3.41	3.06	-0.20	0.00	-13.2	4.6E-06
88	700.1	9.70	10.00	1.00	3.41	3.06	-0.20	-5.00	-12.4	4.6E-06
89	700.1	9.73	10.00	1.00	3.41	3.06	0.00	-5.00	-12.4	4.6E-06
90	800.4	9.89	10.00	1.00	3.82	3.30	0.00	0.00	-13.6	4.6E-06